

Decoupling Control by the Center of Rotation and Gravity Hybrid-Driven Method for High-Precision Scan Stage with Multiple Actuators

Wataru Ohnishi and Hiroshi Fujimoto
The University of Tokyo

5-1-5 Kashiwanoha, Kashiwa, Chiba, 277-8561 Japan
Phone: +81-4-7136-3873, +81-4-7136-4131

Email: ohnishi@hflab.k.u-tokyo.ac.jp, fujimoto@k.u-tokyo.ac.jp

Koichi Sakata, Kazuhiro Suzuki and Kazuaki Saiki
Nikon Corporation

47-1, Nagaodaityou, Sakae, Yokohama, 244-8533 Japan

Email: koichi.sakata@nikon.com

kazuhiro.suzuki@nikon.com

kazuaki.saiki@nikon.com

Abstract—In a multi-input multi-output control system, coupling force between multiple axes can deteriorate control performance and stability. In this paper, a decoupling method utilizing a high-precision stage with multiple actuators is proposed. According to a model considering the misalignment between the center of gravity (CoG), the center of rotation (CoR), the actuation point, and the measurement point, the coupling characteristics from the translational force to the angle can be changed by varying the height of the actuation point. The model indicates that a CoR-driven method can suppress the coupling in the low frequency range and a CoG-driven method can suppress the coupling in the high frequency range. This paper proposes a CoR and CoG hybrid-driven method using complementary filters to place the actuation point at the CoR and the CoG in low and high frequency ranges, respectively. The effectiveness of the proposed method is verified by experiments.

I. INTRODUCTION

High-precision scan stages have an important role in the semiconductor and flat panel display manufacturing processes [1], [2]. To achieve precise positioning accuracy, six degrees of freedom ($x, y, z, \theta_x, \theta_y, \theta_z$) stages with contactless gravity compensation are commonly used [3], [4]. This contactless structure can reduce disturbances such as friction and floor vibration [5]. Because the high-precision stages are multi input multi output (MIMO) systems, the coupling effect can deteriorate the positioning accuracy and productivity.

There are two approaches for decoupling: 1) data based approaches [6], [7], [8], and 2) model based approaches [1], [9], [10]. This paper studies the model based approach. During scanning motion, coupling between the scanning motion (x) and the pitching motion (θ_y) compromises the control performance. One of the reasons for the coupling is a height mismatch of four points on the stage: the center of the gravity (CoG), the center of rotation (CoR), the translational actuation point, and the translational position measurement point [10]. It is difficult to match these four points because of mechanical constraints, such as spatial limitations, and shifts of the CoG due to load mass variations. Moreover, it is hard to estimate the position of the CoG precisely by CAD software analysis because of geometrical tolerances and uncertainties in density

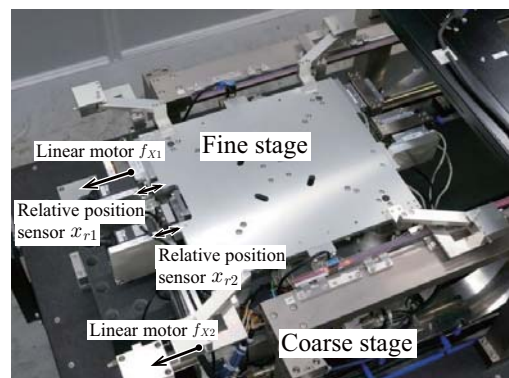
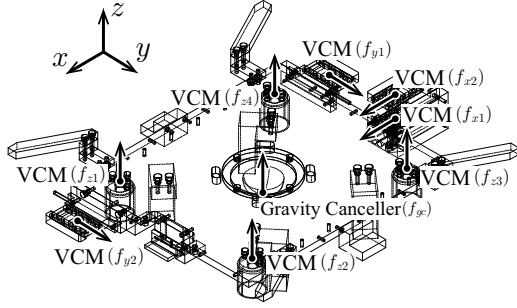


Fig. 1. Experimental setup: 6-DOF high-precision stage.

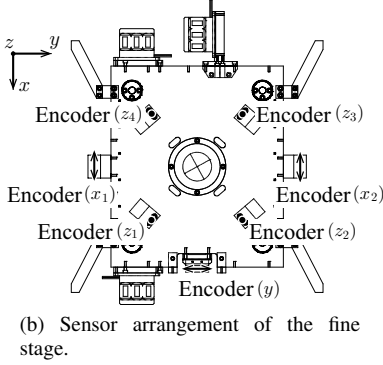
[11], [12].

Our research group proposed a decoupling method consisting of three parts [10]: 1) dual-actuated voice coil motors (VCMs) structured in the x direction that enable us to change the height of the actuation point by means of thrust distribution, 2) a detailed modeling accounting for the misalignment of the CoG, CoR, actuation point, and measurement point, and 3) use of a CoG-driven method and a CoR-driven method. According to model observations, the CoG-driven method, in which the height of the actuation point coincides with the CoG, can reduce the coupling gain from the translational force f_x to the pitching angle θ_y in the high frequency range. On the other hand, the CoR-driven method, in which the height of the actuation point coincides with the CoR, can reduce the coupling gain from f_x to θ_y in the low frequency range. In other words, there is a trade-off between the height of the actuation point and the coupling gain from f_x to θ_y motion.

This paper proposes a CoR and CoG hybrid-driven method, using a complementary filter, to place the actuation point at the CoR and the CoG in low and high frequency ranges, respectively. This method can suppress the coupling from x to θ_y in a wide frequency range. The effectiveness of this method is demonstrated by experiments. The proposed method is based on an idea called integrated design of mechanism and control



(a) Actuator arrangement of the fine stage with two VCMs in x direction.



(b) Sensor arrangement of the fine stage.

Fig. 2. Structure of the fine stage.

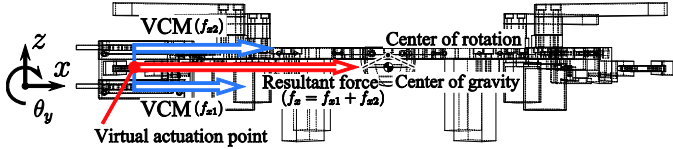
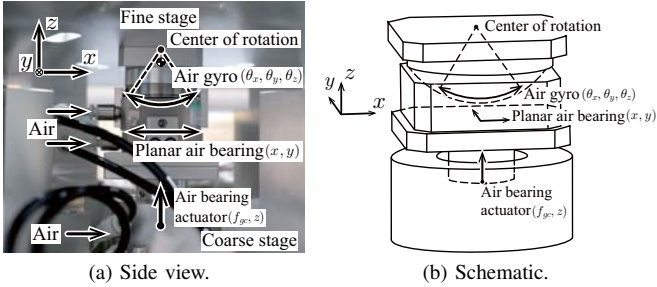


Fig. 3. Side view of the fine stage. By changing the thrust distribution ratio a (see eq. (1) and eq. (2)), the height of the virtual actuation point can be placed arbitrarily.



(a) Side view.

(b) Schematic.

Fig. 4. Structure of the gravity canceller. The radius of the curvature of the air gyro decides the height of the center of rotation (CoR) of the fine stage.

[13], [14], [15].

II. EXPERIMENTAL SETUP

A. Overview

Our research group designed the dual stage shown in Fig. 1. The actuator and sensor arrangement of the fine stage is illustrated in Fig. 2. As shown in Fig. 2(a) and Fig. 3, the fine stage has two VCMs in the x direction.

The fine stage is supported by a 6-DOF air bearing “gravity canceller” [4]. The picture and schematic of the gravity canceller are shown in Fig. 4. The gravity canceller compensates for the gravitational force experienced by the fine stage and supports its 6-DOF without friction. The gravity canceller is composed of three parts: the air gyro, the planar air bearing and the air bearing actuator that support the $(\theta_x, \theta_y, \theta_z)$, (x, y) , and (z) -directional motion, respectively. As shown in Fig. 4, the shape of the air gyro is similar to that of a hemisphere. The fine stage slides on the hemispheric surface of the air gyro with an air gap of a few μm . In this paper, the center of the hemisphere is called the center of rotation (CoR). In other words, the radius of curvature of the air gyro determines the height of the CoR.

B. Changeable actuation point stage by multiple actuators

Due to the spatial limitations of the fine stage, a VCM for the x direction cannot be placed at the desired actuation point. In this section, a new fine stage structure that can shift the virtual actuation point by means of thrust distribution of multiple actuators is introduced. This is based on a simple idea shown in Fig. 3. The two VCMs generate force f_{x1} and f_{x2} in the x direction by a thrust distribution law

$$f_{x1} = af_x, f_{x2} = (1 - a)f_x, \quad (1)$$

where a denotes the thrust distribution ratio. Here, the height of the virtual actuation point L_{fx} is defined as

$$L_{fx} = aL_{fx1} + (1 - a)L_{fx2}, \quad (2)$$

where L_{fx1} and L_{fx2} denote the heights of the actuation point of f_{x1} and f_{x2} from the CoR, respectively.

Although this structure doubles the amount of wiring, and the mass of the fine stage becomes slightly heavier, this structure has advantages, as described below. By changing the thrust distribution ratio a , the height of the virtual actuation point L_{fx} can be placed at the desired point, such as the position of the CoG or the CoR. Moreover, during operation, the CoG shifts as a result of load mass variation. Because the transfer functions depend on the height of the CoG L_{g2} (formulated in (3)–(7)), the coupling characteristics change dynamically. Even in this case, this structure can reduce the coupling forces by means of placing the virtual actuation point at the desired position.

III. MODELING

The model of x and θ_y motion is shown in Fig. 5 and Tab. I. As introduced in section II, this stage has a fixed center of rotation because the stage is supported by the air gyro for $(\theta_x, \theta_y, \theta_z)$. In reference [10], the transfer function from f_x and τ_y to x_m and θ_y is formulated as (3)–(7). Equations (3)–(7) are obtained by following steps: 1) the generalized coordinate definition $q_1 = x_{g1}, q_2 = \theta_y$, 2) Lagrange’s equation formulation, 3) linearization by the following assumptions: $\cos(\theta_y) \approx 1, \sin(\theta_y) \approx \theta_y, \dot{\theta}_y^2 \approx 0$, 4) coordinate transformation to the measurement point. The formulation details are described in reference [10].

$$g_{11}(s) = \frac{x_m(s)}{f_x(s)} = \frac{[J_{\theta_y} + L_{f_x}L_m M_{x1} - (L_{f_x} - L_{g2})(L_{g2} - L_m)M_{x2}]s^2 + (C_{\theta_y} + L_{f_x}L_m C_{x1})s + K_{\theta_y} + L_{f_x}L_m K_{x1} - L_{g2}M_{x2}g}{D(s)} \quad (3)$$

$$g_{21}(s) = \frac{\theta_y(s)}{f_x(s)} = \frac{[L_{f_x}M_{x1} + (L_{f_x} - L_{g2})M_{x2}]s^2 + L_{f_x}C_{x1}s + L_{f_x}K_{x1}}{D(s)} \quad (4)$$

$$g_{12}(s) = \frac{x_m(s)}{\tau_y(s)} = \frac{[L_m M_{x1} + (L_m - L_{g2})M_{x2}]s^2 + L_m C_{x1}s + L_m K_{x1}}{D(s)} \quad (5)$$

$$g_{22}(s) = \frac{\theta_y(s)}{\tau_y(s)} = \frac{(M_{x1} + M_{x2})s^2 + C_{x1}s + K_{x1}}{D(s)} \quad (6)$$

$$D(s) = [(M_{x1} + M_{x2})J_{\theta_y} + M_{x1}M_{x2}L_{g2}^2]s^4 + [(M_{x1} + M_{x2})C_{\theta_y} + (J_{\theta_y} + M_{x2}L_{g2}^2)C_{x1}]s^3 + [(J_{\theta_y} + M_{x2}L_{g2}^2)K_{x1} + (M_{x1} + M_{x2})(K_{\theta_y} - M_{x2}L_{g2}g) + C_{\theta_y}C_{x1}]s^2 + [C_{\theta_y}K_{x1} + C_{x1}(K_{\theta_y} - L_{g2}M_{x2}g)]s + K_{x1}(K_{\theta_y} - L_{g2}M_{x2}g) \quad (7)$$

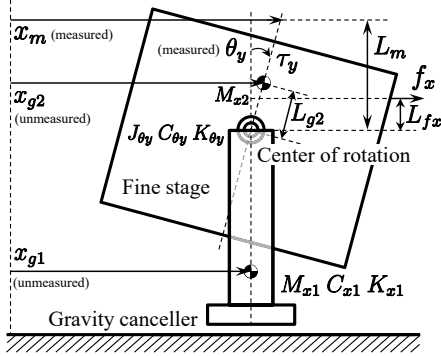


Fig. 5. Fine stage model of the x and θ_y motion. (positive directions of L_{g2} , L_{f_x} and L_m are defined as illustrated)

TABLE I
MODEL PARAMETERS.

Symbol	Meaning	Value
x_m	Measured position of the fine stage	—
x_{g1}	Position of the CoG of the planar air bearing and the air gyro	—
x_{g2}	Position of the CoG of the fine stage	—
θ_y	Measured attitude angle of the fine stage	—
f_x	Input force of the fine stage in the x direction	—
τ_y	Input torque of the fine stage in the θ_y direction	—
M_{x1}	Mass of the planar air bearing and the air gyro	0.077 kg
C_{x1}	Viscosity coefficient in the x_{g1} motion	430 N/(m/s)
K_{x1}	Spring coefficient in the x_{g1} motion	11000 N/m
M_{x2}	Mass of the fine stage	5.3 kg
J_{θ_y}	Moment of inertia of the fine stage	0.10 kgm ²
C_{θ_y}	Viscosity coefficient of the fine stage in the θ_y motion	1.6 Nm/(rad/s)
K_{θ_y}	Spring coefficient of the fine stage in the θ_y motion	1200 Nm/rad
L_m	Distance between the measurement point of x_m and the CoR	-0.028 m
L_{g2}	Distance between the CoR and the CoG of the fine stage	-0.051 m
L_{f_x}	Distance between the CoR of the fine stage and the actuation point	changeable

Equations (4) and (5) suggest that the height mismatch of the CoG, the CoR, the actuation point, and the measurement point causes the coupling effect between x and θ_y motion. In the following section IV, the relationship between the height of the actuation point and coupling characteristics $g_{21}(s)$ is discussed.

IV. DECOUPLING $g_{21}(s)$ USING MULTIPLE ACTUATORS

A. CoG-driven method and CoR-driven method [10]

By changing the actuation point L_{f_x} , equations (3)–(7) suggest that the coupling transfer function $g_{21}(s)$ can be changed without any impact of $g_{12}(s)$ and $g_{22}(s)$. In this section, CoR-driven method and CoG-driven method are introduced [10].

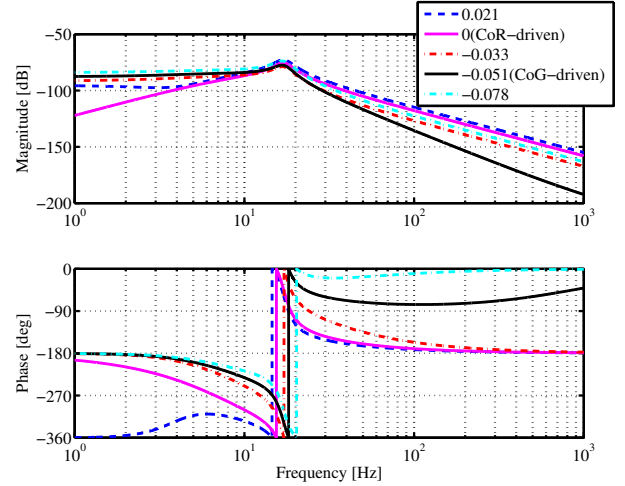


Fig. 6. Frequency characteristics of $g_{21}(s)$ (model parameters are shown in Tab. I). The height of the actuation point L_{f_x} is set as 0.021, 0, -0.033, -0.051, and -0.078. The position of the CoG L_{g2} is fixed as -0.051. There is a trade-off between CoR-driven method ($L_{f_x} = 0$) and CoG-driven method ($L_{f_x} = -0.051$) in high and low frequency ranges.

- CoR-driven method (Fig. 7(a))
If the L_{f_x} is set to 0, this means that the actuation point is placed at the CoR, $L_{f_x}(M_{x1}s^2 + M_{x2}s^2 + C_{x1}s + K_{x1})/D(s)$ becomes 0 in equation (4). In this case, the coupling term $g_{21}(s)$ is only $-L_{g2}M_{x2}s^2/D(s)$. Through this, the coupling gain of $g_{21}(s)$ in low frequencies is suppressed.
- CoG-driven method (Fig. 7(b))
If the L_{f_x} is set as L_{g2} , this means that the actuation point is placed at the CoG, $(L_{g2} - L_{f_x})M_{x2}s^2/D(s)$ becomes 0 in equation (4). In this case, the coupling term is only $L_{f_x}(M_{x1}s^2 + C_{x1}s + K_{x1})/D(s)$. Through this, the coupling gain of $g_{21}(s)$ in high frequencies is suppressed considering $M_{x1} \ll M_{x2}$ (see Tab. I).

The comparison between the CoR- and CoG-driven methods is shown in Fig. 6. Fig. 6 shows that there is a trade-off between the CoR- and CoG-driven methods in low and high frequencies.

B. Proposal of CoR and CoG hybrid-driven method

As described in the subsection IV-A, the coupling characteristics from f_x to θ_y can be changed by the height of the

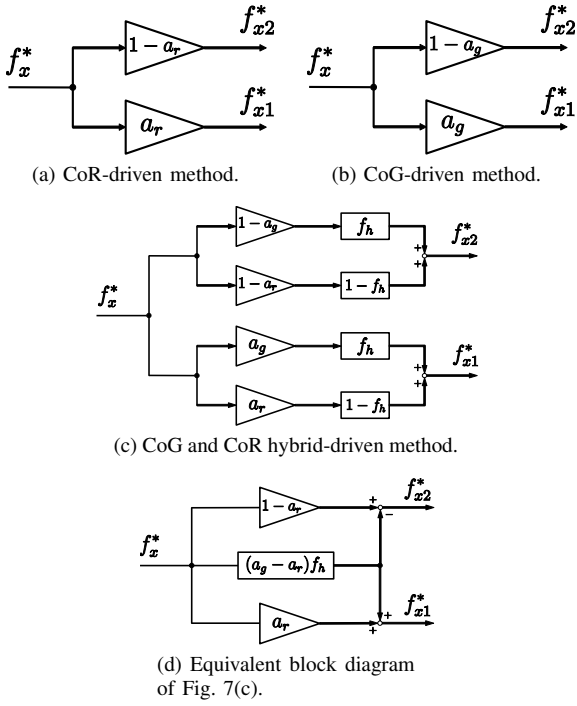


Fig. 7. Block diagram of the thrust distribution described in (1). a_r and a_g denote the thrust distribution constants for CoR-driven method and CoG-driven method, respectively. f_h denotes 1st order high-pass filter to make complementary filter. f_x^* , f_{x1}^* , f_{x2}^* denote the reference of the total force for the x direction, and two VCMs in the x direction shown in Fig. 2(a).

actuation point. However, there is a trade-off shown in Fig. 6.

This paper proposes the CoR and CoG hybrid-driven method. This method can place the actuation height at the CoR in the low frequency range and the CoG in the high frequency range using the 1st order complementary filter illustrated in Fig. 2(a). The cut off frequency of the 1st order complementary filter is set as the break frequency of $g_{21}(s)$.

The Fig. 7(c) configuration needs four high-pass filters $f_h(s)$. However, Fig. 7(c) can also be written as Fig. 7(d) which requires only one high-pass filter.

V. EXPERIMENTS

Experiments are performed by the stage shown in Fig. 1. In the following experiments, the height of the actuation point is changed by the thrust distribution described in the subsection II-B. The height of the actuation point from the CoR is set as $L_{fx} = 0, -0.015, -0.033, -0.051$.

A. Frequency responses

The measured frequency responses are shown in Fig. 8. According to Fig. 8(a), (b), (d), the variation of the actuation height L_{fx} does not affect g_{11}, g_{12}, g_{22} .

Fig. 8(c) indicates that the variation of L_{fx} can change the g_{21} as modeled in section IV and Fig. 6. The hybrid-driven method proposed in the subsection IV-B shows that the CoR and CoG hybrid-driven method can reduce the coupling gain for a wide frequency range as shown in Fig. 8(c).

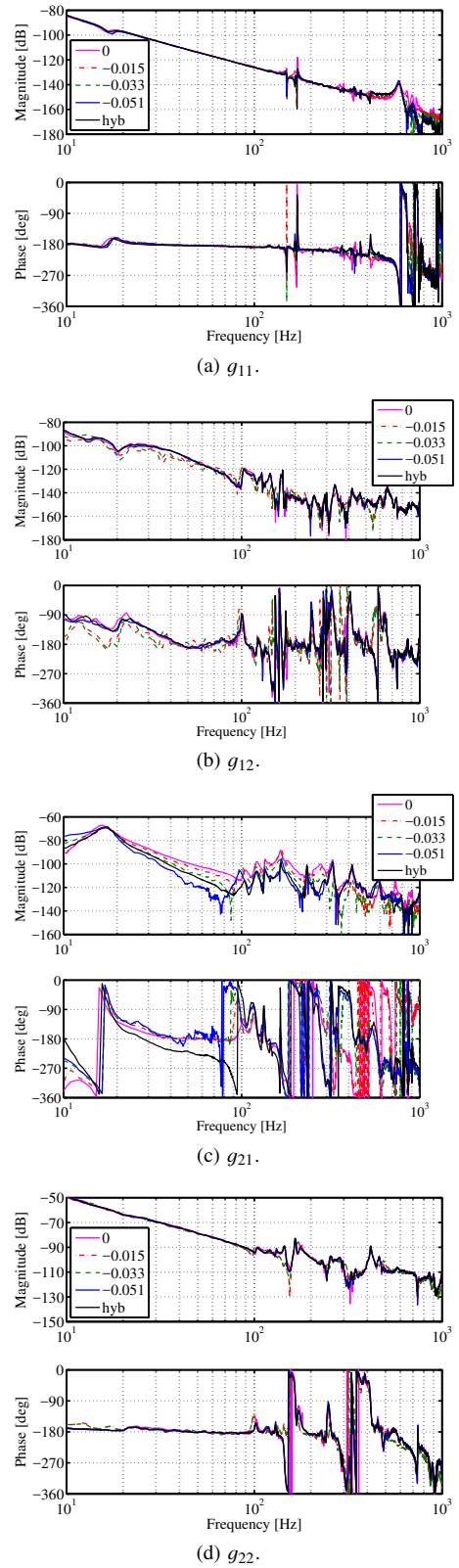


Fig. 8. Measured frequency responses. The height of the actuation point L_{fx} is changed as $0, -0.015, -0.033, -0.051$. “hyb” denotes the hybrid-driven method of $L_{fx} = 0$ and $L_{fx} = -0.051$. Here, the cut off frequency of the $f_h(s)$ is set as 16 Hz. According to Fig. 8(c), there is a trade off between $L_{fx} = 0$ and $L_{fx} = -0.051$ in a high and low frequencies. On the other hand, the hybrid-driven method can reduce the coupling gain.

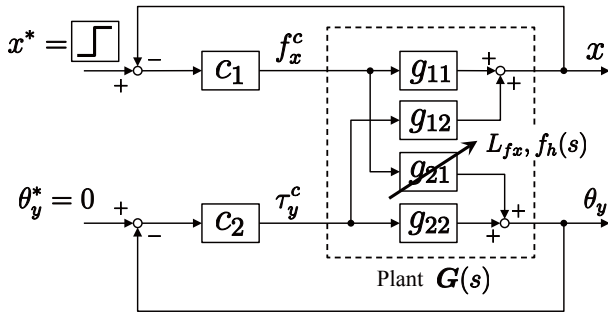


Fig. 9. Block diagram of the step response experiment. The coupling characteristics g_{21} can be shaped by changing the virtual actuation point L_{fx} and the high-path filter $f_h(s)$ of the hybrid-driven method.

B. Time responses

Time responses are measured with the block diagram shown in Fig. 9. Single-input single-output feedback controllers $c_1(s)$, $c_2(s)$ are designed with a pole assignment approach [16], without considering the coupling transfer functions. Designed closed loop poles are at 20 Hz.

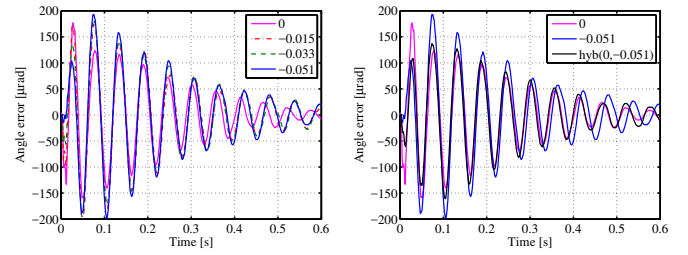
Here, a $100\ \mu\text{m}$ step reference is given for the translational position reference x^* . The reference of the angle θ_y^* is kept at 0 rad. The time responses and maximum error are shown in Fig. 10 and Tab. II, respectively. The figure shows that the CoR and CoG hybrid-driven method can reduce the error generated from coupling dynamics.

VI. CONCLUSION

This paper proposes a center of rotation and gravity hybrid-driven method that accounts for height mismatch of the center of gravity (CoG), the center of rotation (CoR), the actuation point, and the measurement point of the stage. In our previous study [10], the model based analysis suggests that a trade-off exists between the height of the actuation point and the coupling gain from translational force f_x to the pitching angle θ_y . To improve the coupling reduction performance, this paper proposes a CoR and CoG hybrid-driven method, which places the actuation height at the CoR in the low frequency range and at the CoG in the high frequency range. This method requires only one 1st order complementary filter. The effectiveness of the proposed method is verified by frequency and time domain experiments.

REFERENCES

- [1] H. Butler, "Position Control in Lithographic Equipment," *IEEE Control Systems Magazine*, vol. 31, no. 5, pp. 28–47, 2011.
- [2] K. Sakata, H. Asami, K. Hirachi, K. Saiki, and H. Fujimoto, "Self Resonance Cancellation Techniques for a Two-Mass System and Its Application to a Large-Scale Stage," *IEEJ Journal of Industry Applications*, vol. 3, no. 6, pp. 455–462, 2014.
- [3] Y. Choi and D. Gweon, "A high-precision dual-servo stage using halbach linear active magnetic bearings," *IEEE/ASME Transactions on Mechatronics*, vol. 16, no. 5, pp. 925–931, 2011.
- [4] W. Ohnishi, H. Fujimoto, K. Sakata, K. Suzuki, and K. Saiki, "Design and Control of 6-DOF High-Precision Scan Stage with Gravity Canceller," in *American Control Conference*, pp. 997–1002, 2014.
- [5] A. Peijnenburg, J. Vermeulen, and J. van Eijk, "Magnetic levitation systems compared to conventional bearing systems," *Microelectronic engineering*, vol. 83, pp. 1372–1375, 2006.



(a) $L_{fx} = 0, -0.015, -0.033, -0.051$.

(b) $L_{fx} = 0, -0.051$ and hybrid-driven method of $L_{fx} = 0, -0.051$.

Fig. 10. Time responses of θ_y (experimental result of Fig. 9).

TABLE II

MAXIMUM VALUE OF THE ANGLE ERROR OF FIG. 10.

L_{fx}	0	-0.015	-0.033	-0.051	hybrid-driven(0, -0.051)
Error [μrad]	177	195	195	199	161

- [6] M. Heertjes and A. Van Engelen, "Minimizing cross-talk in high-precision motion systems using data-based dynamic decoupling," *Control Engineering Practice*, vol. 19, no. 12, pp. 1423–1432, 2011.
- [7] M. Heertjes, D. Hennekens, and M. Steinbuch, "MIMO feed-forward design in wafer scanners using a gradient approximation-based algorithm," *Control Engineering Practice*, vol. 18, no. 5, pp. 495–506, 2010.
- [8] P. Yang, B. Alamo, and G. Andeen, "Control design for a 6 DOF e-beam lithography stage," in *American Control Conference*, vol. 3, pp. 2255–2260, 2001.
- [9] K. Sakata and H. Fujimoto, "Design Fabrication and Control of 4-DOF High-Precision Stage," in *Proceedings of the 11th IEEE International Workshop on Advanced Motion Control*, pp. 366–370, 2010.
- [10] W. Ohnishi, H. Fujimoto, K. Sakata, K. Suzuki, and K. Saiki, "Proposal of Decoupling Control Method for High-Precision Stages using Multiple Actuators considering the Misalignment among the Actuation Point, Center of Gravity, and Center of Rotation," in *IEEJ International Workshop on Sensing, Actuation, and Motion Control*, 2015.
- [11] V. Melnikov, "Inertia tensors and centres of masses identification at semiprogram precession motions," in *IEEE International Conference on Control Applications*, pp. 494–497, 2012.
- [12] G. Previati, M. Giamiero, and G. Massimiliano, "Advances on Inertia Tensor and Centre of Gravity Measurement: The Intenso+ System," in *68th Annual Conference of Society of Allied Weight Engineers*, 2009.
- [13] A. Hara, K. Saiki, K. Sakata, and H. Fujimoto, "Basic examination on simultaneous optimization of mechanism and control for high precision single axis stage and experimental verification," in *34th Annual Conference of IEEE Industrial Electronics*, pp. 2509–2514, 2008.
- [14] W. Ohnishi, H. Fujimoto, K. Sakata, K. Suzuki, and K. Saiki, "Integrated Design of Mechanism and Control for High-Precision Stages by the Interaction Index in the Direct Nyquist Array Method," in *American Control Conference*, pp. 2825–2830, 2015.
- [15] T. Atsumi, T. Arisaka, T. Shimizu, and H. Masuda, "Head-positioning control using resonant modes in hard disk drives," *IEEE/ASME Transactions on Mechatronics*, vol. 10, no. 4, pp. 378–384, 2005.
- [16] G. C. Goodwin, S. F. Graebe, and M. E. Salgado, *Control System Design*. 2000.